1 **Impact of deoxygenation and hydrological changes on the Black Sea nitrogen cycle during**

2 **the Last Deglaciation and Holocene**

3

4 Anna Cutmore[1*]., Nicole Bale[1]., Rick Hennekam[2]., Bingjie Yang[1]., Darci Rush[1]., Gert-Jan Reichart[2,3]., Ellen C.

5 Hopmans[2]., Stefan Schouten[1,3]

6

7 *[1]Department of Marine Microbiology & Biogeochemistry, NIOZ Royal Netherlands Institute for Sea Research, 1790 AB Den Burg,*

8 *Netherlands*

9 *[2]Department of Ocean Systems, NIOZ Royal Netherlands Institute for Sea Research, 1790 AB Den Burg, Netherlands*

10 *[3]Department of Earth Sciences, Universiteit Utrecht, Princetonlaan 8a, 3584 CB Utrecht, Netherlands*

11 *Corresponding Author: anna.cutmore@nioz.nl

12

13 **Abstract**

14 The marine nitrogen (N) cycle profoundly impacts global ocean productivity. Amid rising deoxygenation in

15 marine environments due to anthropogenic pressures, understanding the impact of this on the marine N-cycle

16 is vital. The Black Sea's evolution from an oxygenated lacustrine basin to an anoxic marine environment over

17 the last deglaciation and Holocene offers insight into these dynamics. Here, we generated records of the organic

18 biomarkers heterocyte glycolipids, crenarchaeol, and bacteriohopanetetrol, associated with various water-

19 column microbial N-cycle processes, which indicate a profound change in Black Sea N-cycle dynamics at ~7.2 ka

20 when waters became severely deoxygenated. This transition substantially reduced Thaumarchaeota-driven

21 nitrification and enhanced loss of bioavailable nitrogen through anammox. In contrast, other climatic changes

22 over the last deglaciation and Holocene, such as freshwater input, water-level variations and temperature

23 changes, did not impact these processes. Cyanobacterial nitrogen fixation in surface waters proved more

24 responsive to changes in salinity and associated water column stratification. Our results indicate that future

25 deoxygenation in marine environments may enhance bioavailable nitrogen loss by anammox and reduce

26 nitrification by Thaumarchaeota, while enhanced stratification may increase cyanobacterial nitrogen fixation in

27 the surface waters.

28

29 **1. Introduction**

30 The marine nitrogen (N) cycle is a significant control of biological productivity in our global oceans. It is directly

31 connected to the fixation of atmospheric carbon dioxide and carbon export from the ocean's surface, influencing

32 atmospheric CO_2 levels over geological time scales (Falkowski et al., 1998). As the marine N-cycle is strongly

33 regulated by biology, the (de)oxygenation of the ocean determines the microorganisms involved in these

34 biogeochemical cycles and the aerobic/anaerobic pathways that occur. Under anoxic conditions, loss of

35 bioavailable nitrogen is substantial, attributed to anaerobic ammonium oxidation (anammox) and denitrification

36 (Kuypers et al., 2003; Dalsgaard et al., 2012). With deoxygenation in marine environments increasing due to

37 anthropogenic climate and environmental changes (i.e., Keeling et al., 2010; Bopp et al., 2013), and research

38 linking deoxygenation to changes in the marine N-cycle (Kalvelage et al., 2013; Naafs et al., 2019), it is important

Climate of the Past Open Access
Discussions
EGU

39 to enhance our understanding of how the marine N-cycle may respond to future deoxygenation and what the

40 associated feedbacks on carbon fixation might be.

41

42 Marine basins that have experienced changes in oxygenation in the past can provide perspective on the current

43 deoxygenation of modern global oceans and the associated feedbacks in the marine N-cycle, in particular on

44 timescales beyond the observational record. Today, the Black Sea is the world's largest permanently stratified

45 anoxic basin with limited connection to the global ocean through the Bosporus Strait and its redox gradient is a

46 hotspot of diverse microbial populations and metabolisms (Kusch et al., 2022). However, over the last

47 deglaciation and Holocene (approximately the last 20 ka), the Black Sea experienced large hydrological changes.

48 The basin was an oxygenated fresh-water lacustrine environment during the Last Glacial Maximum (LGM)

49 (Schrader, 1979) and experienced many environmental changes during the subsequent deglaciation, including

50 temperature changes (Bahr et al., 2005; 2008; Ion et al., 2022), water-level variations (Ivanova et al., 2007;

51 Nicholas et al., 2011; Piper & Calvert, 2011), and changes in freshwater input into the basin, both through

52 melting of Eurasian icesheets and alpine glaciers after the LGM and changes in regional precipitation (Bahr et

53 al., 2005; 2006; 2008; Badertscher et al., 2011; Shumilovskikh et al., 2012). It became reconnected to the global

54 ocean at ~9.6 ka when post-glacial sea-level rise caused an initial marine inflow (IMI) over the Bosporus sill (Aksu

55 et al., 2002; Major et al., 2006; Bahr et al., 2008; Ankindinova et al., 2019), leading to enhanced salinity of the

56 upper part of the water column (Marret et al., 2009; Verleye et al., 2009; Filipova-Marinova et al., 2013) and

57 euxinic deep waters developing in the basin after ~7.2 ka (Arthur & Dean, 1998; Eckert et al., 2013). Thus,

58 sedimentary records of the Black Sea may provide a unique perspective of the impact of deoxygenation, as well

59 as changing temperature and salinity, on the marine N-cycle.

60

61 Diagnostic lipid biomarkers of microbes preserved in the geological record can offer a unique insight into past

62 changes in the N-cycle (Rush & Sinninghe Damsté, 2017 and references cited therein; Elling et al., 2021; van

63 Kemenade et al., 2023). Nitrogen fixing heterocytous cyanobacteria play a crucial role in transforming nitrogen

64 gas (N_2) to bioavailable nitrogen (NH_3) and sustaining primary productivity in both marine and freshwater

65 environments (Villareal, 1992; Ploug et al., 2008). Identification of their diagnostic biomarkers, heterocyte

66 glycolipids (HGs), in the geological record enables exploration of past changes in nitrogen fixation by these

67 microbes (Bauersachs et al., 2009; 2010; Sollai et al., 2017; Bale et al., 2019; Elling et al., 2021). Nitrification, the

68 microbial two-step conversion of ammonia (NH_3) and/or ammonium (NH_4^+) to nitrate (NO_3^-), is a central part of

69 the marine N-cycle. Archaea of the phylum Thaumarchaeota (also known as Nitrososphaerota) are among the

70 most abundant and widespread marine prokaryotes (Karner et al., 2001; Francis et al., 2005), playing a crucial

71 role in nitrification in the Black Sea (Lam et al., 2007) by aerobically oxidizing ammonia to nitrite (Könneke et al.,

72 2005; Wuchter et al., 2006). As Thaumarchaeota are the exclusive producers of the membrane spanning lipid,

73 crenarchaeol (Sinninghe Damste et al., 2002), this biomarker can be used to identify Thaumarchaeota in the

74 geological record and explore the palaeo marine N-cycle. Another critical part of the N-cycle is the loss of

75 bioavailable nitrogen to N_2. Under anoxic conditions, bioavailable nitrogen (NO_3^-, NO_3^-, NH_3 and NH_4^+) can be

76 lost through two processes in subsurface waters: anammox (van de Graaf et al., 1997; Kuypers et al., 2003) and

77   denitrification (Kuenen and Robertson, 1988). It is possible to explore past changes in anammox activity in the

78   sedimentary record using the unique ladderane fatty acids (Sinninghe Damste et al., 2002) but these are

79   relatively poorly preserved in sediments (Jaeschke et al., 2007). Alternatively, the ratio of bacteriohopanetetrol

80   (BHT)-34S (which is ubiquitously synthesized by aerobic bacteria) and the later eluting stereoisomer BHT-x

81   (which is predominately synthesized by marine anammox bacteria, i.e., Ca. Scalindua spp.) (Rush et al., 2014;

82   Schwartz-Narbonne et al., 2020; van Kemenade et al., 2023) can be used to trace past anammox activity.

83   Denitrification is performed by a large range of organisms (Knowles, 1982), but at present, there are no

84   associated diagnostic lipid biomarkers (Rush et al., 2017).

85

86   In this study, we used lipid biomarkers of microbes involved in the N-cycle in combination with other

87   geochemical records from a sediment core located in the western Black Sea spanning the last deglaciation and

88   Holocene (~20 ka – present) to better constrain and assess the sensitivity of the marine N-cycle under changing

89   hydrological and oxygenation conditions and explore its potential links to broader global climate dynamics.

90

91   **2. Regional Setting**

92   The Black Sea is a large meromictic marginal basin connected to the Mediterranean Sea via the Turkish Straits

93   (the Bosporus, the Sea of Marmara, and the Dardanelles Strait) (Fig. 1). The Black Sea has a net outflow into the

94   Aegean Sea via the Turkish Straits, and is primarily supplied by three major rivers, the Danube, Dnieper, and

95   Don. With freshwater flowing out of the basin and dense, highly saline waters flowing in, the water column is

96   highly stratified with respect to salinity (density). An oxygenated colder surface layer (0 – 50 m) overlies warmer,

97   anoxic, sulfidic, hypersaline deep waters (100 – 2300 m), separated by a suboxic layer (50 – 100 m) (Murray et

98   al., 1989; 1995). The general circulation of Black Sea surface-waters is a basin-scale cyclonic boundary current

99   encompassing large eastern and western cyclonic gyres, with several smaller, anticyclonic coastal eddies (Fig. 1)

100   (Özsoy and Ünlüata, 1997).

101

102   **3. Methods**

103   During the cruise with the RV Pelagia in April 2017, piston core 64PE418 (235 cm length) was recovered from

104   1970 m below sea level (mbsl) depth in the Black Sea (42°56 N, 30°02 E) (Fig. 1). 44 sediment samples were taken

105   at 5 cm intervals along the depth of the core.

106

107   *3.1. Biomarker extraction and analysis*

108   Lipids were extracted from these samples using a modified Bligh and Dyer extraction method as described

109   previously (Bale et al., 2021). Using a mixture of methanol (MeOH), dichloromethane (DCM), and phosphate

110   buffer (2:1:0.8, v:v), the sediment was twice extracted ultrasonically (10 min). The combined supernatants were

111   phase-separated by adding DCM and phosphate buffer to create a solvent ratio of 1:1:0.9 (v:v). The organic

112   phase was collected, and the aqueous phase re-extracted three times using DCM. All extraction steps were then

113   repeated on the residue but with a mixture of MeOH, DCM and aqueous trichloroacetic acid solution (TCA) pH

114   3 (2:1:0.8, v:v). Finally, the organic extracts were combined and dried under a N_2 gas stream. A deuterated

115   betaine lipid {1,2-dipalmitoyl-sn-glycero-3-O-4'-[N,N,N-trimethyl(d9)]-homoserine; Avanti Lipids} internal

116   standard was added to each sample before filtering the extract through 0.45 μm cellulose syringe filters (4 mm

117   diameter; BGB, USA). Extraction blanks were performed alongside the sediment extractions, using the same

118   glassware, solvents and extraction methodology, but without sediment. Analysis of the extracts was performed

119   using the following UHPLC-HRMS reversed phase method. An Agilent 1290 Infinity I UHPLC was used, equipped

120   with thermostatted auto-injector and column oven, coupled to a Q Exactive Orbitrap MS with Ion Max source

121   with heated electrospray ionization (HESI) probe (Thermo Fisher Scientific, Waltham, MA). Separation was

122   achieved using an Acquity BEH C18 column (Waters, 2.1 × 150 mm, 1.7 μm) maintained at 30°C. The eluent

123   composition was (A) MeOH/H_2O/formic acid/14.8 M NH_3aq [85:15:0.12:0.04 (v:v)] and (B) IPA/MeOH/formic

124   acid/14.8 M NH_3aq [50:50:0.12:0.04 (v:v)]. The elution program was: 95% A (for 3 min) followed by a linear

125   gradient to 40% A (at 12 min) and then to 0% A (at 50 min), which was maintained until 80 min. The flow rate

126   was 0.2 mL min^{-1}. Positive ion HESI settings were: capillary temperature, 300°C; sheath gas (N_2) pressure, 40

127   arbitrary units (AU); auxiliary gas (N_2) pressure, 10 AU; spray voltage, 4.5 kV; probe heater temperature, 50°C;

128   S-lens 70 V. Lipids were analyzed with a mass range of m/z 350–2000 (resolving power 70,000 ppm at m/z 200),

129   followed by data-dependent tandem MS/MS (resolving power 17,500 ppm), in which the 10 most abundant

130   masses in the mass spectrum were fragmented successively. Optimal fragmentation was achieved with a

131   stepped normalized collision energy of 15, 22.5 and 30 (isolation width, 1.0 m/z) for IPL analysis (Bale et al.,

132   2021) and 22.5 and 40 (isolation width 1.0 m/z) for BHP analysis (Hopmans et al., 2021). The Q Exactive was

133   calibrated within a mass accuracy range of 1 ppm using the Thermo Scientific Pierce LTQ Velos ESI Positive Ion

134   Calibration Solution. During analysis, dynamic exclusion was used to temporarily exclude masses (for 6 s) to

135   allow selection of less abundant ions for MS/MS.

136

137   Biomarkers were identified based on their retention time, exact mass, and fragmentation spectra. Integrations

138   were performed on (summed) mass chromatograms of relevant molecular ions ([M+H]$^+$, [M+NH4]$^+$, and

139   [M+Na]$^+$) and in the case of crenarchaeol also the second isotope peak for each of the three adducts. Due to

140   coelution of BHT-34S, BHT-x isomer and an unknown nitrogen containing compound with the same mass,

141   identification and integration of BHT-34S and BHT-x was conducted using the m/z 529.462 dehydrated insource

142   product ([M+H]$^+$-H_2O). Isoprenoidal glycerol dialkyl glycerol tetraether (isoGDGT) crenarchaeol, monohexose

143   crenarchaeol, and a crenarchaeol isomer were all integrated and combined as 'crenarchaeol'. The lipid

144   biomarker records are all presented as peak area per gram of total organic carbon (TOC).

145

146   **3.2. Total organic carbon and total nitrogen and $\delta^{15}N_{bulk}$ measurements**

147   Freeze-dried sediments were analysed for TOC, total nitrogen (TN) and bulk $\delta^{15}N$ ($\delta^{15}N_{bulk}$) using a

148   ThermoScientific Flash EA Delta V Plus IRMS. Flow was 100 ml/min and the temperature for oxidation, reduction

149   and the oven were 900°C, 680°C, and 40°C, respectively. Nitrogen isotopic measurements were calibrated to

150   atmospheric air (AIR) and values are expressed in permil (‰) units. Inorganic carbon was removed from the

151   sediment prior to TOC analysis using HCl (2 mol), cleaned with bi-distilled water, then freeze-dried.

152

3.3. Age model

154 Accelerator Mass Spectrometry (AMS) ^{14}C ages of bulk organic matter were measured from core 64PE418 (n =
155 7) to create a chronology on the 64PE418 depth scale. Samples were weighed and freeze-dried at NIOZ. The
156 AMS ^{14}C measurements (^{14}C/ [12]C) were determined using a Compact Carbon AMS System at the Poznań
157 Radiocarbon Laboratory, Poland. The sediment samples were pre-treated with 0.25M HCl (room temperature
158 overnight, then 80°C, 1+ hour), and rinsed with deionised water until pH = 7. Samples were then combusted in
159 closed (sealed under vacuum) quartz tubes, together with CuO and Ag wool (900°C, 10 hours). The CO_2 released
160 was then dried in a vacuum line and reduced with H_2 using 2 mg of iron (Fe) powder as a catalyst. The obtained
161 carbon and Fe mixture was then pressed into an aluminium holder (Czernik & Goslar, 2001). The measurement
162 was performed by comparing intensities of ionic beams of ^{14}C, ^{13}C and ^{12}C measured for each sample and for
163 standard samples (with "Oxalic Acid II" used as modern standard; "coal" used as background standard of [14]C-
164 free carbon). In each AMS run, 30-33 samples of unknown age were measured, alternated with measurements
165 of 3-4 samples of modern standard and 1-2 samples of background standard. The measured ^{14}C/ [12]C ratios are
166 corrected for isotopic fractionation and reported as conventional radiocarbon age according to Stuiver & Polach
167 (1977).

168

169 Seven bulk organic matter ^{14}C dates were used in the production of the age-model for core 64PE418 (Table 1
170 and Fig. S3). Six of these were from this core, with an additional bulk organic carbon ^{14}C date from the widely
171 acknowledged Unit I/II boundary of core KNR 134-08 BC17, which was used to further refine the age model for
172 the upper part of the core (Jones & Gagnon, 1994). Core KNR 134-08 BC17 was sourced from the same location
173 and water depth as 64PE418 and this boundary was identified in our core using the same significant colour and
174 elemental changes described in previous studies (Fig. S1 & S2) (i.e., Arthur & Dean, 1998; Bahr et al., 2005).
175 While seven ^{14}C measurements were conducted on core 64PE418, one was excluded from the age model due to
176 an age reversal (142.5 cm), likely due to the presence of reworked material. Variable reservoir-ages were added
177 to our calibration (Table 1), using those calculated by Kwiecien et al., (2008) for intermediate water depths in
178 the Black Sea over the last deglaciation and Holocene. The ^{14}C dates were calibrated using the Marine20
179 calibration curve (Heaton et al., 2020) for the upper three samples (24.5, 39, 76.5 cm) which reflect the period
180 after the infiltration of marine water; this is based on the colour and elemental changes in the core which
181 indicate that these samples fall within Units I and II (Arthur & Dean, 1998; Bahr et al., 2005). The lower four
182 samples (118.5, 158.5, 183.5 and 217.5 cm) were calibrated using the IntCal20 calibration curve (Reimer et al.,
183 2020), as they reflect the period prior to the marine infiltration when then Black Sea was a lacustrine
184 environment, as indicated by colour and elemental signatures in the core (Arthur & Dean, 1998; Bahr et al.,
185 2005). Using the R-code CLAM (Blaauw, 2010), the age–depth model was created based on the seven ^{14}C dates.
186 Our age model shows that the 64PE418 biomarker records span the last 19.5 ka, with an average resolution of
187 ~450 years. The following transitions are identified in our core by colour (Fig. S1) and elemental changes (Fig.
188 S2) and dated by our age model as follows: the onset of the IMI (138 cm) is at 9.6 ka ± 237 yrs, the boundary of
189 Unit II/III (96 cm) is dated at 7.2 ka ± 202 yrs, and the Unit I/II boundary (39 cm) is dated at 2.6 ka ± 402 yrs. The

190   dates of these boundaries align well with previously published calibrated ages for these transitions (i.e., Jones

191   & Gagnon, 1994; Ankindinova et al., 2019; Huang et al., 2021), as shown in Fig. S4.

192

193   **4. Results**

194

195   ***4.1. TOC, TN and colour changes***

196   Sedimentary bulk TOC (%), bulk TN (%), and $\delta^{15}N_{bulk}$ (‰) range between 0.3 – 22.8% for TOC and 0.05 – 1.9% for

197   TN, and 5.2 – 0.0‰ for $\delta^{15}N_{bulk}$ (Fig. 2). There are significant colour changes in the core, as shown in Fig. S1 which

198   correspond to changes in TOC, TN and the elemental composition (Fig. S2). In the lower part of the core (19.5 –

199   9.6 ka), values are relatively low for TOC and TN, at ~0.84% and ~0.10%, respectively. At 9.6 ka, there is an

200   appreciable change in the elemental composition of the core, with increases in Ti/Ca, K and V and a decrease in

201   Mn/Al, which corresponds with a transition to darker sediments and an increase in TOC and TN to ~2.41% and

202   ~0.26%, respectively. At 7.2 ka there is another major change in the colour and bulk elemental composition of

203   the core, with an increase in redox-sensitive elements U, V, and Mo and a decrease in Ti/Ca and K (Fig. S2), which

204   corresponds with darker sediments and increasing TOC values. TOC peaks between 6.6 – 4.6 ka (~21% for TOC

205   and ~1.7% for TN), declining towards the top of the core. $\delta^{15}N_{bulk}$ shows a general decline in values from the

206   upper to the lower part of the core. This decline is small between 19.5 – 7.7 ka (4.9 – 3.3‰), before a more

207   significant decrease to 1.2‰ at 6.6 ka (3.3 – 1.2‰). Values increase to 3.7‰ at 6.1 ka before declining to 0.0‰

208   at 3.9 ka, increasing slightly towards the top of the core to values of 1.3‰.

209

210   ***4.2. Biomarkers***

211   We examined a number of lipid biomarkers related to the N-cycle in Black Sea core 64PE418 (Fig. S2). HGs were

212   identified in all samples (with the exception of 215 cm (16.4 ka)). These include HGs with a hexose (C_6) headgroup

213   i.e., hexose C_{26} diol, hexose C_{28} diol, hexose C_{28} triol and hexose C_{30} triol, which are specific to free-living

214   cyanobacteria, found in predominately freshwater and brackish environments (Bauersachs et al, 2009; Wörmer

215   et al., 2012). In addition, those with a pentose (C_5) headgroup i.e., pentose C_{30} diol, pentose C_{30} triol, pentose

216   C_{32} triol were detected which are specific to cyanobacteria symbiotic with diatoms (diatom-diazotroph

217   associations, DDAs) (Schouten et al., 2013; Bale et al., 2015). Hexose HGs are present throughout the core,

218   increasing substantially in abundance between 9.6 – 6.6 ka, reaching maximum values at 9.6 ka. Pentose HGs

219   are detected from 4.3 ka onwards, increasing in abundance at the top of the record coinciding with low

220   abundance of hexose HGs. Crenarchaeol, a marker for Thaumarchaeota, was identified throughout our record,

221   showing high values in the early part of the record (~ 1.1E+14 peak area per g TOC) until 6.9 ka, abruptly shifting

222   to lower values ~ 3.9E+13 peak area per g TOC thereafter. The BHT-x ratio, a biomarker for anammox bacteria,

223   is low in the early part of our record (<0.3), due to low abundance of BHT-x. The BHT-x ratio increases after 6.9

224   ka to values around 0.3, due to higher abundance of BHT-x and lower abundance of BHT with a 34S

225   stereoconfiguration.

226

227 Finally, to reconstruct levels of oxygen in the subsurface waters of the Black Sea, isorenieratene was identified

228 (as described in Bale et al., 2021). Isorenieratene is a marker of the brown-coloured strains of the photosynthetic

229 green sulfur bacteria, Chlorobiaceae, which are anoxygenic photoautotrophs that require light and hydrogen

230 sulphide (H_2S); their presence indicates photic zone euxinia, whereby anoxic, sulfidic waters reached the photic

231 zone (Sinninghe Damste et al., 1993; Koopmans et al., 1996). Isorenieratene was identified in many of our

232 samples after 9.5 ka, peaking between 5.6 – 4.3 ka (reaching 3.39E+12 per g TOC at 5.6 ka), but was not detected

233 between 3.9 – 2.7 ka.

234

235 **5. Discussion**

236 Based on clear changes in TOC (Fig. 2), colour and elemental signatures (Fig. S1 & S2), we divided core 64PE418

237 into three widely acknowledged units, in line with previous studies (Jones & Gagnon, 1994; Arthur & Dean, 1998;

238 Bahr et al., 2005). Unit III spans ~20 – 7.2 ka, covering the period where the Black Sea was a lacustrine

239 environment, disconnected from the global ocean, and also the transition interval, where the basin moved

240 towards a marine environment after the IMI over the Bosporus sill at ~9.6 ka (Aksu et al., 2002; Major et al.,

241 2006; Bahr et al., 2008; Ankindinova et al., 2019). Unit II (~7.2 – 2.6 ka) and Unit I (~2.6 ka - present) span the

242 period where the Black Sea had become an anoxic brackish-to-marine environment.

243

244 **5.1. Oxic lacustrine phase (19.5 – 9.6 ka)**

245 Throughout the last deglaciation and early Holocene (19.5 – 9.6 ka), TOC and TN levels are low, likely due to

246 poor preservation of organic material, caused by the well-ventilated, oxygenated, freshwater environment that

247 existed in the basin at this time (Schrader, 1979). Isorenieratene is not detected during this period, while

248 elements that accumulate in sediment under anoxic conditions (i.e., Algeo and Li, 2020) also remained low (i.e.,

249 U, V, Mo; see Fig. S2), which all points to a well-oxygenated environment. Freshwater/brackish conditions

250 prevailed throughout this time, as shown by previous studies (Fig. S5; Filipova-Marinova et al., 2013; Ion et al.,

251 2022; Huang et al., 2022).Throughout this period, the abundance of Thaumarchaeota, indicated by crenarchaeol

252 abundance, and anammox, indicated by the BHT-x ratio, remained relatively steady. This stability is remarkable

253 since the region experienced significant climatic changes which led to large variations in the surface water

254 temperatures of the Black Sea, varying from ~10°C during the Bølling Allerød, ~7°C during the Younger Dryas

255 and ~14°C by the Early Holocene (Ménot & Bard, 2012), as well as changes in the input of freshwater into the

256 basin due regional precipitation variability and the melting of Eurasian icesheets and alpine glaciers (Bahr et al.,

257 2005; 2006; 2008; Badertscher et al., 2011; Shumilovskikh et al., 2012; Filipova-Marinova et al., 2013; Ion et al.,

258 2022). In contrast, changes in HG abundance and distribution suggest that surface-dwelling nitrogen-fixing

259 cyanobacteria were sensitive to hydrological changes in the Black Sea over this period (Fig. 3). The dominant HG

260 structure varies between hexose C_{26} diol, hexose C_{28} diol and hexose C_{30} triol and after 11 ka, hexose C_{28} triol

261 becomes present, which has been shown to be the major HG in members of the Rivulariaceae family (i.e.,

262 Calothix sp.) (Bauersachs et al., 2009). The warmer wetter conditions of the Early Holocene may have provided

263 a trigger for this change in HG abundance and composition. Indeed, an increase in the abundance of the

264 genus *Rivularia* was also noted in coastal regions of SW India during this period, coinciding with an increasingly

265 warm and wet climate (Limaye et al., 2017). Another cause for this shift may have been related to changes in

266 nutrient availability, with members of the Rivulariaceae family typically occurring in environments with highly

267 variable phosphorus availability (Whitton & Mateo, 2012).

268

269 **5.2. Transition phase (9.6 – 7.2 ka)**

270 In line with existing research (Arthur & Dean, 1998; Bahr et al., 2006; 2008), the IMI occurred at ~9.6 ka, leading

271 to a significant change in colour (Fig. S1) and elemental composition of the sedimentary record (Fig. S2), as well

272 as a substantial increase in abundance of HGs. This increase does not coincide with higher TOC content,

273 suggesting that enhanced preservation of HGs was not the cause. It is possible that these lipid biomarkers were

274 transported fluvially to this site from lakes within the catchment basin of the Black Sea due to the warm/wet

275 conditions at this time (Göktürk et al., 2011; Shumilovskikh et al., 2012; Filipova-Marinova et al., 2013). This,

276 however, appears unlikely as our site is located a substantial distance from the mouths of major rivers (>230

277 km), and the BIT index remains low during this period (~0.08; pers. comms. B.Yang), indicating only a minor

278 contribution of terrestrial organic matter at our site (Hopmans et al., 2004). Furthermore, as the proceeding

279 period (7 – 5.6 ka) was also warm and wet (Göktürk et al., 2011; Shumilovskikh et al., 2012; Filipova-Marinova

280 et al., 2013), we would expect the continuation of this peak if the HGs were being sourced from surrounding

281 lacustrine environments. Instead, these high values decline abruptly after 6.6 ka.

282

283 It is therefore likely that the peak abundance in nitrogen-fixing cyanobacteria is related to warmer Black Sea

284 surface temperatures during the early to mid-Holocene (Bahr et al., 2008) in combination with surface water

285 stratification (Bahr et al., 2006). This stratification may have been driven in part by enhanced freshwater influx

286 due to wetter conditions but may also have been triggered by the IMI through the Bosporus Strait at ~9.6 ka

287 (Major et al., 2006; Bahr et al., 2008; Ankindinova et al., 2019). This IMI likely led to the gradual salinisation of

288 the water column over this transition interval and intermittent build-up of anoxia in the water column. This, in

289 turn, led to periods of higher preservation of organic matter compared to the preceding period, as indicated by

290 the slight increase in TOC after 9.6 ka. The presence of isorenieratene after 9.4 ka indicates that anoxia reached

291 the photic zone at intermittent periods during this transition interval, thereby providing sufficient conditions for

292 the presence of the anoxygenic photoautotrophs, Chlorobiaceae. While the peak in nitrogen-fixing

293 cyanobacteria occurs ~2 ka before anoxia intermittently entered the photic zone, the initial influx of dense saline

294 water may have led to some reduction in vertical circulation, which reduced the amount of fixed nitrogen

295 upwelled to the upper water column, leading to the presence of nitrogen-fixing cyanobacteria at 9.6 ka. This

296 also coincides with a change in the distribution of HGs in our record between 9.7 – 6.9 ka where hexose C_{28} diol

297 and hexose C_{30} triol increase in abundance and hexose C_{28} triol declines in relative abundance and is no longer

298 present after 9.1 ka, coinciding with the presence of isorenieratene. These changes may reflect a shift in species

299 composition, linked to the gradual salinisation and periodic anoxification of the water column after the IMI. The

300 IMI at ~9.6 ka appears, however, to have had little impact on the abundances of anammox and Thaumarchaeota.

301 This is possibly because basin-wide water column stratification and the permanent build-up of anoxia did not

302 occur until later in the record, meaning that neither process instantaneously reacted to the IMI at ~9.6 ka.

Climate
of the Past
Discussions

5.3. Shift to anoxic brackish-to-marine mode of operation: a critical N-cycle threshold (~7.2 ka to present)

After 7.2 ka there was a substantial increase in TOC and TN and an abrupt shift in parts of the subsurface N-cycle. The latter is shown by an increase in the BHT-x ratio, indicating an intensification of anammox, which is coeval with a decrease in crenarchaeol, indicating that there was a decline in Thaumarchaeota-driven nitrification. Studies have shown that by ~7.2 ka anoxia had built up in the water column, as indicated by changes in redox elements (Fig. S2 and Eckert et al., 2013; Wegwerth et al., 2018) and water column salinity had significantly increased (Fig. S5; Hiscott et al., 2007; Marret et al., 2009; Soulet et al., 2011; Filipova-Marinova et al., 2013), following the IMI from the Sea of Marmara at ~9.6 ka (Major et al., 2002; 2006; Bahr et al., 2005; 2008; Ankindinova et al., 2019). This is supported by the presence of isorenieratene in our record during this time, which indicates that anoxia penetrated the photic zone. This water column anoxia likely led to the enhanced preservation of TOC and TN and triggered a shift in the subsurface N-cycle, which crossed a threshold from an oxygenated lacustrine mode of operation to an anoxic brackish-to-marine mode of operation. The anoxic water column enabled anammox bacteria to expand their habitat from the anoxic sediments, where they likely were confined when the basin was an oxygenated freshwater environment, up into the suboxic/anoxic water column. This may therefore have commenced part of the modern-day N-cycle in the Black Sea where anammox activity occurs in the lower suboxic zone (~100 mbsl) where O_2 is (near) depleted and H_2S is absent (Jensen et al., 2008), with anammox bacteria consuming ammonium diffusing from the deep sea and utilising the nitrite produced by both Thaumarchaeota and ammonia-oxidising bacteria (AOB) (Kuypers et al., 2003; Lam et al., 2007). Consequently, it may be that the abundance of anammox bacteria increased as a result of the coupling to nitrite production by other microbes in the suboxic zone, whilst benefitting from ammonium diffusing upwards from the deep sea. The increased anammox after 7.1 ka likely indicates that more bioavailable nitrogen was lost from the system after the switch to the anoxic brackish-to-marine mode of operation. At the same time, Thaumarchaeota abundance declined, which may be in part due to the build-up of anoxia in the water column which reduced the niche of these aerobic microbes and the nitrification performed by them. Once these processes crossed a threshold from an oxygenated lacustrine mode of operation to an anoxic brackish-to-marine mode of operation, they appear to have remained steady for the remainder of the Holocene despite changes in the salinity of the basin (van der Meer et al., 2008; Mertens et al., 2012; Coolen et al., 2013) and significant changes in regional temperature and precipitation (Göktürk et al., 2011; Shumilovskikh et al., 2012; Filipova-Marinova et al., 2013). This shows that deoxygenation was the main driver of the observed change in annammox as well as archaeal nitrification and that they were not affected by hydrological changes mainly occurring at the surface.

At 6.1 ka, the abundance of the HGs substantially declined, coinciding with an increase in $\delta^{15}N_{bulk}$, indicating a reduction in nitrogen fixation. As this decline in HG abundance and increase in $\delta^{15}N_{bulk}$ does not coincide with a reduction in TOC, it is unlikely that reduced preservation of HGs played a role here. As nitrogen-fixing cyanobacteria inhabit the upper surface layer, it is likely that this change is linked to the salinisation of the surface waters, with many studies demonstrating the disappearance of many freshwater mollusc, ostracod and

341 dinoflagellate cyst species at this time, which were replaced by an increased abundance of euryhaline

342 Mediterranean species (Hiscott et al., 2007; Marret et al., 2009; Filipova-Marinova et al., 2013; Ivanova et al.,

343 2015). At 6.1 ka, hexose C_{26} diol and hexose C_{28} diol are the only HGs present in the record, which may reflect

344 the dominance of genera in the Nostocaceae family (i.e., Anabaena sp., Aphanizomenon sp., Nodularia sp.,

345 Nostoc sp.), as these members demonstrate a dominance of the hexose C_{26} diol and also contain varying

346 amounts of hexose C_{28} diol (Gambacorta et al., 1999; Bauersachs et al., 2009). This distribution is similar to that

347 of the Baltic Sea after ~7.2 ka when a series of weak intrusions of saline water led to the basin becoming fully

348 brackish (Sollai et al., 2017). It is therefore possible that the peak in HGs in our Black Sea record between 9.6 –

349 6.9 ka represents a transition from the dominance of freshwater tolerant nitrogen-fixing cyanobacteria to more

350 brackish species, with brackish species dominating the surface-waters after 6.6 ka. After 6.1 ka, $\delta^{15}N_{bulk}$ gradually

351 decreases, indicating a rise in nitrogen fixation, as shown in previous studies (Blumenberg et al., 2009; Fulton et

352 al., 2012). It should be noted that a previous study has suggested, based on compound specific measurements

353 of pyropheophytin, that sedimentary $\delta^{15}N$ in the Black Sea is primarily derived from eukaryotic algae rather than

354 cyanobacteria (Fulton et al., 2012), meaning the use of $\delta15N_{bulk}$ as a nitrogen fixation signal must be used with

355 caution. HGs, however, are only derived from N-fixing cyanobacteria and are therefore an unambiguous

356 biomarker of nitrogen fixation. Interestingly, at 4.3 ka pentose HGs are detected, coinciding with lowest $\delta^{15}N_{bulk}$,

357 indicating the presence of marine nitrogen-fixing cyanobacteria found in symbiosis with marine diatoms. This

358 indicates that the surface water salinity had reached a threshold which enabled these marine microbes to

359 survive, with research indicating salinity reached ~17‰ during the deposition of Unit I (Ion et al., 2022) and

360 freshwater/brackish species had disappeared by this time (Fig. S5; Filipova-Marinova et al., 2013). Indeed,

361 reported increases in the number of euryhaline species at this time also points to the increasing salinity of the

362 surface waters (Marret et al., 2009; Bradley et al., 2012), which may be linked to warmer/drier conditions which

363 reduced freshwater influx and/or enhanced evaporation (Göktürk et al., 2011). Between 3.9 – 2.7 ka,

364 isorenieratene is not detected in the samples, reflecting the findings of previous studies (Sinninghe Damsté et

365 al., 1993). It has been suggested that this resulted from the erosion of the chemocline (Sinninghe Damsté et al.,

366 1993), while other research shows a short reoccurrence of freshwater/brackish species (Fig. S5; Filipova-

367 Marinova et al., 2013), which may indicate that enhanced freshwater input was responsible for lowering the

368 chemocline below the photic zone. The disappearance of hexose HGs after 0.6 ka indicates that surface water

369 salinities may more recently have become too high for the proliferation of brackish nitrogen-fixing

370 cyanobacteria.

371

372 **6. Conclusions**

373 This study shows a relatively stable subsurface N-cycle in the Black Sea over the last deglaciation and Holocene

374 with the exception of a critical threshold observed at 7.2 ka when the basin shifted from an oxygenated

375 lacustrine environment to an anoxic brackish-to-marine basin. At this time, the loss of bioavailable nitrogen

376 through anammox activity was enhanced and Thaumarchaeota-driven nitrification was reduced. Prior to, and

377 after this transition, the subsurface N-cycle was remarkably stable despite various climatic and hydrological

378 changes that impacted the basin during the deglaciation and Holocene periods. Both the amount of nitrogen

379 fixation by cyanobacteria and the composition of these microbes in the surface waters, however, appear to be
380 much more dynamic and sensitive to hydrological changes over this period, responding in particular to salinity
381 and temperature changes and stratification of the water column. Consequently, these records provide
382 important insight into how future deoxygenation and stratification in marine environments may affect the
383 microorganisms involved in the N-cycle. While deoxygenation in marine environments may lead to enhanced
384 loss of bioavailable nitrogen by anammox, and reduced nitrification by Thaumarchaeota, enhanced stratification
385 of the water column may lead to enhanced cyanobacterial nitrogen fixation in the surface waters. These changes
386 may have associated feedbacks on nutrient cycling and carbon fixation, with implications for the future global
387 carbon budget.

388

389 **Data Availability**

390 All data generated for this study are archived and publicly available via the Mendeley Data repository online at
391 https://10.17632/4c9fg7jf5d.1 (Cutmore et al., 2024).

392

400

401 **Author Contributions**

402 Anna Cutmore: Conceptualization, Formal analysis, Investigation, Data Curation, Visualization, Writing - Original
403 Draft, Writing - Review & Editing; Nicole Bale: Conceptualization, Methodology, Investigation, Supervision,
404 Writing - Review & Editing; Rick Hennekam: Resources, Formal analysis, Investigation, Writing - Review & Editing;
405 Darci Rush: Formal analysis, Writing - Review & Editing; Bingjie Yang: Formal analysis, Investigation, Writing -
406 Review & Editing; Gert-Jan Reichart: Resources, Supervision, Writing - Review & Editing; Ellen C. Hopmans:
407 Supervision; Stefan Schouten: Conceptualization, Supervision, Funding acquisition, Writing - Review & Editing

408

409 **Competing interests:** The authors declare that they have no conflict of interest.

410

411 **References:**

412

413 Aksu, A., Hiscott, R.N., Kaminski, M.A., Mudie, P.J., Gillespie, H., Abrajano, T and Yasar, D. 2002. Last glacial–
414 Holocene paleoceanography of the Black Sea and Marmara Sea: stable isotopic, foraminiferal and coccolith
415 evidence. *Marine Geology*, **190**, 119-149. doi.org/10.1016/S0025-3227(02)00345-6

416

417   Algeo, T.J and Li, C. 2020. Redox classification and calibration of redox thresholds in sedimentary systems.

418   *Geochimica et Cosmochimica Acta*, **287**, 8-26. doi.org/10.1016/j.gca.2020.01.055

419

420   Ankindinova, O., Hiscott, R.N., Aksu, A.E and Grimes, V. 2019. High-resolution Sr-isotopic evolution of Black Sea

421   water during the Holocene: Implications for reconnection with the global ocean. *Marine Geology*, **407**, 213-228.

422   doi.org/10.1016/j.margeo.2018.11.004

423

424   Arthur & Dean, 1998. Organic-matter production and preservation and evolution of anoxia in the Holocene Black

425   Sea. *Palaeoceanography & Palaeoclimatology,* **13**, 395-411. doi.org/10.1029/98PA01161

426

427   Badertscher, S., Fleitmann, D., Cheng, H., Edwards, R.L., Göktürk, O.M., Zumbühl, A., Leuenberger, M and Tüysüz,

428   O. 2011. Pleistocene water intrusions from the Mediterranean and Caspian seas into the Black Sea. *Nature*

429   *Geoscience*, **4**, 236–239. doi.org/10.1038/ngeo1106

430

431   Bale, N., Hopmans, E.C., Zell, C., Sobrinho, R.L., Kim, J.-H., Sinninghe Damsté, J.S., Villareal, T.A and Schouten, S.

432   2015. Long chain glycolipids with pentose head groups as biomarkers for marine endosymbiotic heterocystous

433   cyanobacteria. *Organic Geochemistry*, **81**, 1-7. doi.org/10.1016/j.orggeochem.2015.01.004

434

435   Bale, N.J., Hennekam, R., Hopmans, E.C., Dorhout, D., Reichart, G.-J., van der Meer, M.T.J., Villareal, T.A.,

436   Sinninghe Damsté, J.S and Schouten, S. 2019. Biomarker evidence for nitrogen-fixing cyanobacterial blooms in a

437   brackish surface layer in the Nile River plume during sapropel deposition. *Geology*, **47**, 1088–1092.

438   doi.org/10.1130/G46682.1

439

440   Bale, N., Ding, S., Hopmans, E.C., Arts, M.G.I., Villanueva, L., Boschman, C., Haas, A.F., Schouten, S and Sinninghe

441   Damsté, J.S. 2021. Lipidomics of Environmental Microbial Communities. I: Visualization of Component

442   Distributions Using Untargeted Analysis of High-Resolution Mass Spectrometry Data. Frontiers in Microbiology,

443   **12**, 1-15. doi.org/10.3389/fmicb.2021.659302

444

445   Bahr, A., Lamy, F., Arz, H., Kuhlmann, H and Wefer, G. 2005. Late glacial to Holocene climate and sedimentation

446   history in the NW Black Sea. *Marine Geology*, **214**, 309-322. doi.org/10.1016/j.margeo.2004.11.013

447

448   Bahr, A., Arz, H., Lamy, F and Wefer, G. 2006. Late glacial to Holocene paleoenvironmental evolution of the Black

449   Sea, reconstructed with stable oxygen isotope records obtained on ostracod shells. *Earth and Planetary Science*

450   *Letters Volume*, **241**, 863-875. doi.org/10.1016/j.epsl.2005.10.036

451

452   Bahr, A., Lamy, F., Arz, H., Major, C., Kwiecien, O and Wefer, G. 2008. Abrupt changes of temperature and water

453   chemistry in the late Pleistocene and early Holocene Black Sea. *Geochemistry, Geophysics, Geosystems*, **9**, 1-16.

454   http://doi.org/10.1029/2007GC001683

455

456 Bauersachs, T., Compaoré, J., Hopmans, E.C., Stal, L.J., Schouten, S and Sinninghe Damsté, J. 2009. Distribution
457 of heterocyst glycolipids in cyanobacteria. *Phytochemistry*, **70**, 2034-2039.
458 doi.org/10.1016/j.phytochem.2009.08.014

459

460 Bauersachs, T., Speelman, E.N., Hopmans, E.C., Reichart, G.-J., Schouten, S and Sinninghe Damsté, J. 2010.
461 Fossilized glycolipids reveal past oceanic N2 fixation by heterocystous cyanobacteria. *Earth & Planetary Science*
462 *Letters*, **107**, 19190-19194. doi.org/10.1073/pnas.1007526107

463

464 Blaaw, M. 2010. Methods and code for 'classical' age-modelling of radiocarbon sequences. *Quaternary*
465 *Geochronology*, **5**, 512-518. doi.org/10.1016/j.quageo.2010.01.002

466

467 Blumenberg, M., Seifert, R., Kasten, S., Bahlmann, E and Michaelis, W. 2009. Euphotic zone bacterioplankton
468 sources major sedimentary bacteriohopanepolyols in the Holocene Black Sea. *Geochimica et Cosmochimica*
469 *Acta*, **73**, 750-766. doi.org/10.1016/j.gca.2008.11.005

470

471 Bopp, L., Resplandy, L., Orr, J.C., Doney, S.C., Dunne, J.P., Gehlen, M., Halloran, P., Heinze, C., Ilyina, T., Séférian,
472 R., Tjiputra, J and Vichi, M. 2013. Multiple stressors of ocean ecosystems in the 21st century: projections with
473 CMIP5 models. *Biogeosciences*, **10**, 6225–6245. doi.org/10.5194/bg-10-6225-2013

474

475 Bradley, L.R., Marret, F., Mudie, P. J., Aksu, A.E and Hiscott, R. N. 2012. Constraining Holocene sea-surface
476 conditions in the south-western Black Sea using dinoflagellate cysts. *Journal of Quaternary Science*, **27**, 835-843.
477 doi.org/10.1002/jqs.2580

478

479 Coolen, M.J.L., Orsib, W.D., Balkema, C., Quince, C., Harris, K., Sylva, S.P., Filipova-Marinova, M and Giosan, L.
480 2013. Evolution of the plankton paleome in the BlackSea from the Deglacial to Anthropocene. *PNAS*, **110**, 8609–
481 8614. doi.org/10.1073/pnas.1219283110

482

483 Czernik, J and Goslar, T. 2001. Preparation of Graphite Targets in the Gliwice Radiocarbon Laboratory for AMS
484 14C Dating. *Radiocarbon*, **43**, 283–291. doi.org/10.1017/S0033822200038121

485

486 Dalsgaard, T., Thamdrup, B., Farías, L and Revsbech, N.P. 2012. Anammox and denitrification in the oxygen
487 minimum zone of the eastern South Pacific. *Limnology & Oceanography*, **57**, 1331-1346.
488 doi.org/10.4319/lo.2012.57.5.1331

489

490 Eckert, S., Brumsack, H.-J., Severmann, S., Schnetger, B., März, C and Fröllje, H. 2013. Establishment of euxinic
491 conditions in the Holocene Black. *Geology*, **41**, 431–434. doi.org/10.1130/G33826.1

492

Climate
of the Past
Discussions

493   Elling, F.J., Hemingway, J.D., Kharbush, J.J., Becker, K.W., Polik, C.A and Pearson, A. 2021. Linking diatom-
494   diazotroph symbioses to nitrogen cycle perturbations and deep-water anoxia: Insights from Mediterranean
495   sapropel events. *Earth and Planetary Science Letters*, **571**, 1-11. doi.org/10.1016/j.epsl.2021.117110

497   Falkowski, P.G., Barber, R.T and Smetacek, V. 1998.Biogeochemical controls and feedbacks on ocean primary
498   production. *Science*, **281**, 200-206. doi.org/10.1126/science.281.5374.20

500   Filipova-Marinova, M., Pavlov, D., Coolen, M and Giosan, L. 2013. First high-resolution marinopalynological
501   stratigraphy of Late Quaternary sediments from the central part of the Bulgarian Black Sea area. *Quaternary*
502   *International*, **293**, 170-183. doi.org/10.1016/j.quaint.2012.05.002

504   Francis, C.A., Roberts, K.J., Beman, J.M., Santoro, A.E., Oakley, B.B. 2005. Ubiquity and diversity of ammonia-
505   oxidizing archaea in water columns and sediments of the ocean. *Proceedings of the National Academy of*
506   *Sciences of the USA*, **102**, 14683-14688. doi.org/10.1073/pnas.050662510

508   Fulton, J.M., Arthur, M.A and Freeman, K.H. 2012. Black Sea nitrogen cycling and the preservation of
509   phytoplankton δ15N signals during the Holocene. *Global Biogeochemical Cycles*, **26**, 1-15.
510   doi.org/10.1029/2011GB004196

512   Gambacorta, A., Trincone, A., Soriente, A and Sodano, G. 1999. Chemistry of glycolipids from the heterocysts of
513   nitrogen-fixing cyanobacteria. *Phytochemistry*, **2**, 145–150.

515   Göktürk, O.M., Fleitmann, D., Badertscher, S., Cheng, H., Edwards, R.L., Leuenberger, M., Fankhauser, A., Tüysüz,
516   O and Kramers, J. 2011. Climate on the southern Black Sea coast during the Holocene: implications from the
517   Sofular Cave record. *Quaternary Science Reviews*, **30**, 2433-2445. doi.org/10.1016/j.quascirev.2011.05.007

519   Heaton, T.J., Köhler, P., Butzin, M., Bard, E., Reimer, R.W., Austin, W.E.N., Bronk Ramsey, C., Grootes, P.M.,
520   Hughen, K.A., Kromer, B., Reimer, P.J., Adkins, J., Burke, A., Cook, M.S., Olsen, J and Skinner, L.C. 2020.
521   Marine20—The Marine Radiocarbon Age Calibration Curve (0–55,000 cal BP). *Radiocarbon*, **62**, 779–820.
522   doi.org/10.1017/RDC.2020.68

524   Hiscott, R.N., Aksu, A.E., Mudie, P.J., Marret, F., Abrajano, T., Kaminski, M.A., Evans, J., Çakiroğlu, A.İ., Yaşar, D.
525   2007. A gradual drowning of the southwestern Black Sea shelf: Evidence for a progressive rather than abrupt
526   Holocene reconnection with the eastern Mediterranean Sea through the Marmara Sea Gateway. *Quaternary*
527   *International*, **167–168**, 19-34. doi.org/10.1016/j.quaint.2006.11.007
528

Climate
of the Past
Discussions

529 Hopmans, E.C., Weijers, J.W.H., Schefuß, E., Herfort, L., Sinninghe Damsté, J.S and Schouten, S. 2004. A novel

530 proxy for terrestrial organic matter in sediments based on branched and isoprenoid tetraether lipids. *Earth and*

531 *Planetary Science Letters*, **224**, 107-116. doi.org/10.1016/j.epsl.2004.05.012

532

533 Hopmans, E.C., Smit, N.T., Schwartz-Narbonne, R., Sinninghe Damste, J.S and Rush, D. 2021. Analysis of non-

534 derivatized bacteriohopanepolyols using UHPLC-HRMS reveals great structural diversity in environmental lipid

535 assemblages. *Organic Geochemistry*, **160**, 1-17. doi.org/10.1016/j.orggeochem.2021.104285

536

537 Huang, Y., Zheng, Y., Heng, P., Giosan, L and Coolen, M.J.L. 2021. Black Sea paleosalinity evolution since the last

538 deglaciation reconstructed from alkenone-inferred Isochrysidales diversity. *Earth and Planetary Science Letters*,

539 **564**, 1-9. doi.org/10.1016/j.epsl.2021.116881

540

541 Ion, G., Briceag, A., Vasiliu, D., Lupaşcu, N and Melinte-Dobrinescu, M. 2022. A multiproxy reconstruction of the

542 Late Pleistocene-Holocene paleoenvironment: New insights from the NW Black Sea. *Marine Geology*, **443**, 1-19.

543 doi.org/10.1016/j.margeo.2021.106648

544

545 Ivanova, E.V., Murdmaa, I.O., Chepalyga, A.L., Cronin, T.M., Pasechnik, I.V., Levchenko, O.V., Howe, S.S.,

546 Manushkina, A.V and Platonova, E.A. 2007. Holocene sea-level oscillations and environmental changes on the

547 Eastern Black Sea shelf. *Palaeogeography, Palaeoclimatology, Palaeoecology*, **246**, 228-259.

548 doi.org/10.1016/j.palaeo.2006.09.014

549

550 Ivanova, E.V., Marret, F., Zenina, M.A., Murdmaa, I.O., Chepalyga, A.L., Bradley, L.R., Schornikov, E.I., Levchenko,

551 O.V and Zyryanova, M.I. 2015. The Holocene Black Sea reconnection to the Mediterranean Sea: New insights

552 from the northeastern Caucasian shelf. *Palaeogeography, Palaeoclimatology, Palaeoecology*, **427**, 41-61.

553 doi.org/10.1016/j.palaeo.2015.03.027

554

555 Jaeschke, A., Hopmans, E. C., Wakeham, S. G., Schouten, S and Sinninghe Damsté, J.S. 2007. The presence of

556 ladderane lipids in the oxygen minimum zone of the Arabian Sea indicates nitrogen loss through anammox.

557 *Limnology and Oceanography*, **52**, 780–786. doi.org/10.4319/lo.2007.52.2.0780

558

559 Jensen, M.M., Kuypers, M.M.M., Lavik, G and Thamdrup, B. 2008. Rates and regulation of anaerobic ammonium

560 oxidation and denitrification in the Black Sea. *Limnology and Oceanography*, **53**, 23-36.

561 doi.org/10.4319/lo.2008.53.1.0023

562

563 Jones, G.A and Gagnon, A.R. 1994. Radiocarbon chronology of Black Sea sediments. *Deep-Sea Research 1*, **41**,

564 531-557. doi.org/10.1016/0967-0637(94)90094-9

565

566   Kalvelage, T., Lavik, G., Lam, P., Contreras, S., Arteaga, L., Löscher, C.R., Oschlies, A., Paulmier, A., Stramma, L
567   and Kuypers, M.M.M. 2013. Nitrogen cycling driven by organic matter export in the South Pacific oxygen
568   minimum zone. *Nature Geoscience*, **6**, 228-234. doi.org/10.1038/ngeo1739

570   Karner, M. B., DeLong, E. F., Karl, D. M. 2001. Archaeal dominance in the mesopelagic zone of the Pacific Ocean.
571   *Nature*, **409**, 507–510. doi.org/10.1038/35054051

573   Keeling, R.F., Körtzinger, A and Gruber, N. 2010. Ocean Deoxygenation in a Warming World. *Annual Review of*
574   *Marine Science*, **2**, 199-229. doi.org/10.1146/annurev.marine.010908.163855.

576   Knowles, R. 1982. Denitrification. *Microbiological Reviews*, **46**, 43-70. doi.org/10.1128/mr.46.1.43-70.1982.

578   Könneke, M., Bernhard, A.E., de la Torre, J.R., Walker, C.B., Waterbury, J.B and Stahl, D.A. 2005. Isolation of an
579   autotrophic ammonia-oxidizing marine archaeon. *Nature*, **437**, 543–546. doi.org/10.1038/nature03911

581   Koopmans, M.P., Köster, J., Van Kaam-Peters, H.M.E., Kenig, F., Schouten, S., Hartgers, W.A., de Leeuw, J.W and
582   Sinninghe Damsté, J.S. 1996. Diagenetic and catagenetic products of isorenieratene: Molecular indicators for
583   photic zone anoxia. *Geochimica et Cosmochimica Acta*, **60**, 4467-4496. doi.org/10.1016/S0146-6380(97)00025-
584   9

586   Kuenen, J.G and Robertson, L.A. 1988. Ecology of nitrification and denitrification. *In:* Cole, J.A and Ferguson, S.J
587   (eds.), The Nitrogen and Sulphur Cycles. Cambridge University Press, Cambridge, pp. 161-218.

589   Kusch, S., Wakeham, S.G and Sepúlveda, J. 2022. Bacteriohopanepolyols across the Black Sea redoxcline trace
590   diverse bacterial metabolisms. *Organic Geochemistry*, **172**, 1-18. doi.org/10.1016/j.orggeochem.2022.104462

592   Kuypers, M.M.M., Sliekers, A.O., Lavik, G., Schmid, M., Barker Jørgensen, B., Kuenen, J.G., Sinninghe Damsté,
593   J.S., Strous, M and Jetten, M.S.M. 2003. Anaerobic ammonium oxidation by anammox bacteria in the Black Sea.
594   Nature, 422, 608-611. doi.org/10.1038/nature01472

596   Kwiecien, O., Arz, H.W., Lamy, F., Wulf, S., Bahr, A., Röhl, U and Haug, G.H. 2008. Estimated Reservoir Ages of
597   the Black Sea Since the Last Glacial. *Radiocarbon*, 50, 99-118. doi.org/10.1017/S0033822200043393

599   Lam, P., Jensen, M.M., Lavik, G., McGinnis, D.F., Müller, B., Schubert, C.J., Amann, R., Thamdrup, B., and Kuypers,
600   M.M.M. 2007. Linking crenarchaeal and bacterial nitrification to anammox in the Black Sea. *PNAS*, **104**, 7104-
601   7109. doi.org/10.1073/pnas.061108110
602

603   Limaye, R.B., Padmalal, D and Kumaran, K.P.N. 2017. Cyanobacteria and testate amoeba as potential proxies for

604   Holocene hydrological changes and climate variability: Evidence from tropical coastal lowlands of SW India.

605   *Quaternary International*, **443**, 99-114. doi.org/10.1016/j.quaint.2016.09.044

606

607   Major, C., Ryan, W., Lericolais, G and Hajdas, I. 2002. Constraints on Black Sea outflow to the Sea of Marmara

608   during the last glacial–interglacial transition. Marine Geology, 190, 19-34. doi.org/10.1016/S0025-

609   3227(02)00340-7

610

611   Major, C., Goldstein, S., Ryan, W., Lericolais, G., Piotrowski, A.M and Hajdas, I. 2006. The co-evolution of Black

612   Sea level and composition through the last deglaciation and its paleoclimatic significance. *Quaternary Science*

613   *Reviews*, **25**, 2031-2047. doi.org/10.1016/j.quascirev.2006.01.032

614

615   Marret, F., Mudie, P., Aksu, A and Hiscott, R.N. 2009. A Holocene dinocyst record of a two-step transformation

616   of the Neoeuxinian brackish water lake into the Black Sea. *Quaternary International*, **197**, 72-86.

617   doi.org/10.1016/j.quaint.2007.01.010

618

619   Ménot, G and Bard, E. 2012. A precise search for drastic temperature shifts of the past 40,000 years in

620   southeastern Europe. *Palaeoceanography*, **27**, 1-13. doi.org/10.1029/2012PA002291

621

622   Mertens, K.N., Bradley, L.R., Takano, Y., Mudie, P.R., Marret, F., Aksu, A.E., Hiscott, R.N., Verleye, T.J., Mousing,

623   E.A., Smyrnova, L.L., Bagheri, S., Mansor, M., Pospelova, V and Matsuoka, K. 2012. Quantitative estimation of

624   Holocene surface salinity variation in the Black Sea using dinoflagellate cyst process length. *Quaternary Science*

625   *Reviews*, **39**, 45-59. doi.org/10.1016/j.quascirev.2012.01.026

626

627   Murray, J.W., Jannasch, H. W., Honjo, S., Anderson, R. F., Reeburgh, W. S., Top, Z., Friederich, G. E., Codispoti, L.

628   A and Izdar, E. 1989. Unexpected changes in the oxic/anoxic interface in the Black Sea. *Nature*, **337**, 411-413.

629   doi.org/10.1038/338411a0

630

631   Murray, J.W., Codispoti, L.A and Friederich, G.E. 1995. Oxidation-reduction environments: the suboxic zone in

632   the Black Sea. *In:* Huang C.P., O'Melia C.R., Morgan J.J. (Eds) Aquatic Chemistry: Interfacial and Interspecies

633   Processes. ACS Advances in Chemistry Series. No. 224. pp. 157-176. doi.org/10.1021/ba-1995-0244.ch007

634

635   Naafs, B.D.A., Monteiro, F.M., Pearson, A., Higgins, M.B., Pancost, R.D and Ridgwell, A. 2019. Fundamentally

636   different global marine nitrogen cycling in response to severe ocean deoxygenation. *Proceedings of the National*

637   *Academy of Sciences*, **116**, 24979-24984. doi.org/10.1073/pnas.1905553116

638

Climate
of the Past
Discussions

639   Nicholas, W.A., Chivas, A.R., Murray-Wallace, C.V and Fink, D. 2011. Prompt transgression and gradual

640   salinisation of the Black Sea during the early Holocene constrained by amino acid racemization and radiocarbon

641   dating. *Quaternary Science Reviews*, **30**, 3769-3790. doi.org/10.1016/j.quascirev.2011.09.018

642

643   Özsoy, E and Ünlüata, Ü. 1997. Oceanography of the Black Sea: A review of some recent results. *Earth Science*

644   *Reviews*, **42**, 231-272. doi.org/10.1016/S0012-8252(97)81859-4

645

646   Piper, D.Z and Calvert, S.E. 2011. Holocene and late glacial palaeoceanography and palaeolimnology of the Black

647   Sea: Changing sediment provenance and basin hydrography over the past 20,000 years. *Geochimica et*

648   *Cosmochimica Acta*, **75**, 5597-5624. doi.org/10.1016/j.gca.2011.07.016

649

650   Ploug, H. 2008. Cyanobacterial surface blooms formed by Aphanizomenon sp. and Nodularia spumigena in the

651   Baltic Sea: Small-scale fluxes, pH, and oxygen microenvironments. *Limnology & Oceanography*, **53**, 914-921.

652   doi.org/10.4319/lo.2008.53.3.0914

653

654   Reimer, P.J., Austin, W.E.N., Bard, E., Bayliss, A., Blackwell, P.G., Bronk Ramsey, C., Butzin, M., Cheng, H.,

655   Edwards, R.L., Friedrich, N., Grootes, P.M., Guilderson, T.P., Hajdas, I., Heaton, T.J., Hogg, A.G., Hughen, K.A.,

656   Kromer, B., Manning, S.W., Muscheler, R., Palmer, J.G., Pearson, C., van der Plicht, J., Reimer, R.W., Richards,

657   D.A., Scott, E.M., Southon, J.R., Turney, C.S.M., Wacker, L., Adolphi, F., Büntgen, U., Capano, M., Fahrni, S.M.,

658   Fogtmann-Schulz, A., Friedrich, R., Köhler, P., Kudsk, S., Miyake, F., Olsen, J., Reinig, F., Sakamoto, M., Sookdeo,

659   A and Talamo, S. 2020. The IntCal20 Northern Hemisphere Radiocarbon Age Calibration Curve (0–55 cal kBP).

660   *Radiocarbon*, **62**, 725–757. doi.org/10.1017/RDC.2020.41

661

662   Rush, D., Sinninghe Damsté, J.S., Poulton, S.W., Thamdrup, B., Garside, A.L., Acuña González, J., Schouten, S.,

663   Jetten, M.S.M and Talbot, H.M. 2014. Anaerobic ammonium-oxidising bacteria: A biological source of the

664   bacteriohopanetetrol stereoisomer in marine sediments. *Geochimica et Cosmochimica Acta*, **140**, 50-64.

665   doi.org/10.1016/j.gca.2014.05.014

666

667   Rush, D and Sinninghe Damsté, J.S. 2017. Lipids as paleomarkers to constrain the marine nitrogen cycle.

668   *Environmental Microbiology*, **19**, 2119-2132. doi.org/10.1111/1462-2920.13682

669

670   Schouten, S., Hopmans, E.C and Sinninghe Damsté, J.S. 2013. The organic geochemistry of glycerol dialkyl

671   glycerol tetraether lipids: A review. *Organic Geochemistry*, **54**, 19-61.

672   doi.org/10.1016/j.orggeochem.2012.09.006

673

674   Schrader, H.-J. 1979. Quaternary Paleoclimatology of the Black Sea basin. *Sedimentary Geology*, **23**, 165-180.

675   doi.org/10.1016/0037-0738(79)90013-7

676

677   Schwartz-Narbonne, N., Schaeffer, P., Hopmans, E.C., Schenesse, M., Charlton, E.A., Jones, D.M., Sinninghe
678   Damsté, J.S., Farhan, M., Haque, U., Jetten, M.S.M., Lengger, S.K., Murrell, J.C., Normand, P., Nuijten, G.H.L.,
679   Talbot, H.M and Rush, D. 2020. A unique bacteriohopanetetrol stereoisomer of marine anammox. *Organic*
680   *Geochemistry*, **143**, 1-10. doi.org/10.1016/j.orggeochem.2020.103994
681
682   Shumilovskikh, L.S., Tarasov, P., Arz, H.W., Fleitmann, D., Marret, F., Nowaczyk, N., Plessen, B., Schlütz, F and
683   Behling, H., 2012. Vegetation and environmental dynamics in the southern Black Sea region since 18 kyr BP
684   derived from the marine core 22-GC3. *Palaeogeography, Palaeoclimatology, Palaeoecology*, **337–338**, 177-193.
685   doi.org/10.1016/j.palaeo.2012.04.015
686
687   Sinninghe Damste, J.S., Wakeham, S.G., Kohnen, M.E.L., Hayes, J.M., de Leeuw, J.W. 1993. A 6,000–year
688   sedimentary molecular record of chemocline excursions in the Black Sea. *Nature*, **362**, 827–829.
689   doi.org/10.1038/362827a0
690
691   Sinninghe Damsté, J.S., Schouten, S., Hopmans, E.C., van Duin, A.C.T and Geenevasen, A.J.A. 2002. Crenarchaeol.
692   *Journal of Lipid Research*, **43**, 1641-1651.
693
694   Sollai, M., Hopmans, E.C., Bale, N.J., Mets, A., Warden, L., Moros, M and Sinninghe Damsté, J.S. 2017. The
695   Holocene sedimentary record of cyanobacterial glycolipids in the Baltic Sea: an evaluation of their application
696   as tracers of past nitrogen fixation. *Biogeosciences*, **14**, 5789–5804. doi.org/10.5194/bg-14-5789-2017
697
698   Soulet, G., Ménot, G., Lericolais, G and Bard, E. 2011. A revised calendar age for the last reconnection of the
699   Black   Sea   to   the   global   ocean.   *Quaternary   Science   Reviews*,   **30**,   1019-1026.
700   doi.org/10.1016/j.quascirev.2011.03.001
701
702   Stuiver, M and Polach, H.A. 1977. Discussion Reporting of 14C Data. *Radiocarbon*, **19**, 35-363. doi.org/
703   10.1017/S0033822200003672
704
705   van de Graaf, A.A., de Bruijn, P., Robertson, L.A., Jetten, M.S.M and Kuenen, J.G. 1997. Metabolic pathway of
706   anaerobic ammonium oxidation on the basis of 15N studies in a fluidized bed reactor. *Microbiology*, **143**, 2415–
707   2421. doi.org/10.1099/00221287-143-7-2415
708
709   van der Meer, M.J.M., Sangiorgi, F., Baas, M., Brinkhuis, H., Sinninghe Damsté, J.S and Schouten, S. 2008.
710   Molecular isotopic and dinoflagellate evidence for Late Holocene freshening of the Black Sea. *Earth and*
711   *Planetary Science Letters*, **267**, 426-434. doi.org/10.1016/j.epsl.2007.12.001
712
713   van Kemenade, Z.R., Cutmore, A., Hennekam, R., Hopmans, E.C., van der Meer, M.T.J., Mojtahid, M., Jorissen,
714   F.J., Bale, N.J., Reichart, G.-J., Sinninghe Damsté, J.S and Rush, D. 2023. Marine nitrogen cycling dynamics under

715 altering redox conditions: insights from deposition of sapropels S1 and the ambiguous S2 in the Eastern

716 Mediterranean Sea. *Geochimica et Cosmochimica Acta*, **354**. doi.org/10.1016/j.gca.2023.06.018

717

718 Verleye, T.J., Mertens, K.N., Louwye, S and Arz, H.W. 2009. Holocene salinity changes in the southwestern black

719 sea: A reconstruction based on dinoflagellate cysts. *Palynology*, **33**, 77-100.

720

721 Villareal, T.A. 1992. Marine Nitrogen-Fixing Diatom-Cyanobacteria Symbioses. *In:* Carpenter, E.J., Capone, D.G

722 and Rueter, J. G (eds.), Marine Pelagic Cyanobacteria: Trichodesmium and other Diazotrophs.

723 Springer:Dordrecht, pp. 163-175.

724

725 Wegwerth, A., Eckert, S., Dellwig, O., Schnetger, B., Severmann, S., Weyer, S., Brüske, A., Kaiser, J., Köster, J.,

726 Arz, H.W and Brumsack, H.-J. 2018. Redox evolution during Eemian and Holocene sapropel formation in the

727 Black Sea. *Palaeogeography, Palaeoclimatology, Palaeoecology*, **489**, 249-260.

728

729 Whitton, B.A and Mateo, P. 2012. Rivulariaceae. In: Whitton, B.A (ed.), Ecology of Cyanobacteria II.

730 Springer:Dordrecht, pp. 561–591. doi.org/10.1007/978-94-007-3855-3_22

731

732 Wörmer, L., Cires, S., Velazquez, D., Quesada, A and Hinrichs, K.-U. 2012. Cyanobacterial heterocyst glycolipids

733 in cultures and environmental samples: Diversity and biomarker potential. *Limnology & Oceanography*, **57**,

734 1775-1788. doi.org/10.4319/lo.2012.57.6.1775

735

736 Wuchter, C., Abbas, B., Coolen, M.J.L., Herfort, L., van Bleijswijk, J., Timmers, P., Strous, M., Teira, E., Herndl,

737 G.J., Middelburg, J.J., Schouten, S and Sinninghe Damsté, J.S. 2006. Archaeal nitrification in the ocean. *PNAS*,

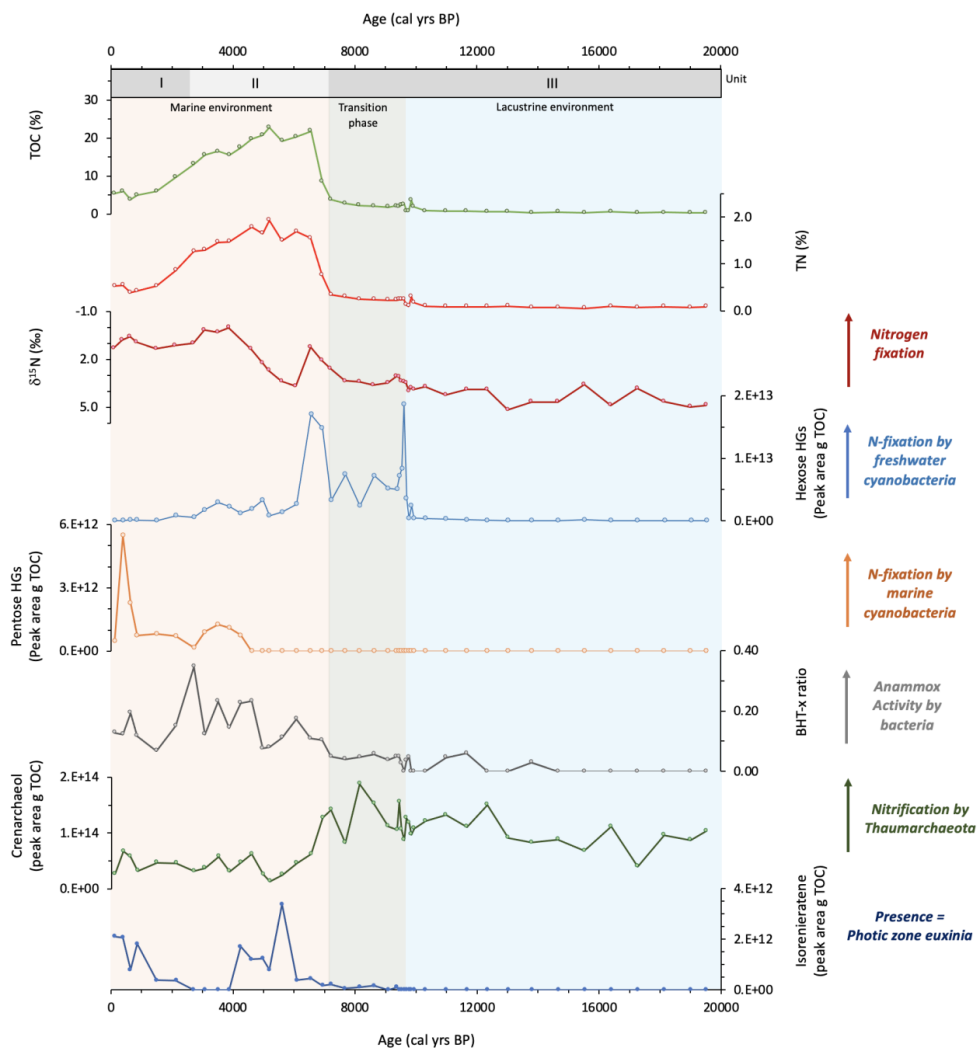738 **103**, 12317-12322. doi.org/10.1073/pnas.0600756103

739

740

741
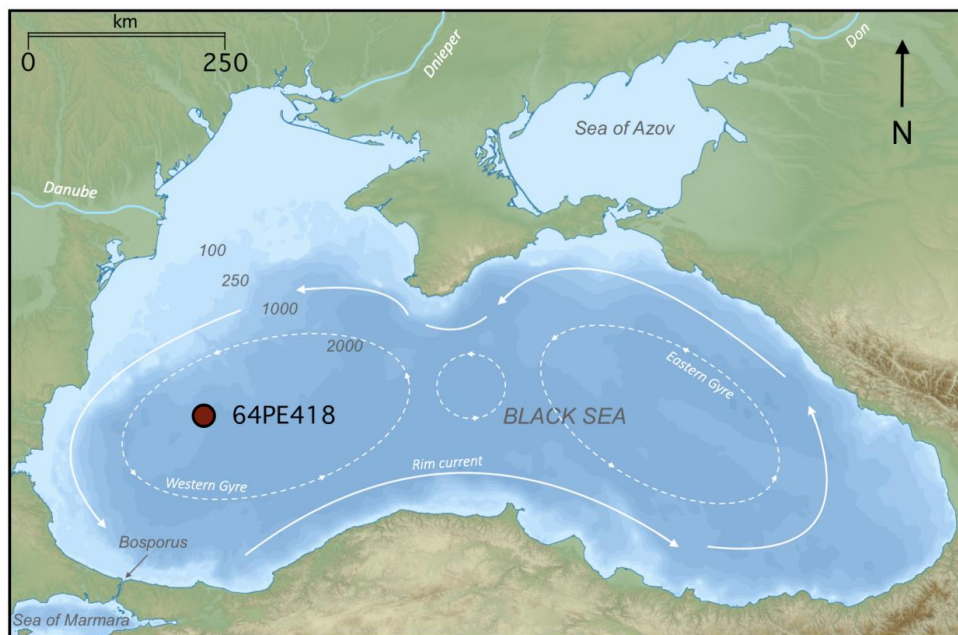
Figure 1: Map of the Black Sea basin, showing the major surface circulation and location of core 64PE418. (Adapted from: Giorgi Balakhadze, English Wikipedia, 2016).

Figure 2: Geochemical records from Black Sea core 64PE418 of: a) TOC (%); b) TN (%); c) $\delta^{15}N_{bulk}$ (‰); d) hexose HGs (peak area per g TOC); e) pentose HGs (peak area per g TOC); f) BHT-x ratio; g) crenarchaeol (peak area per g TOC); h) isorenieratene (peak area per g TOC).

Figure 3: Changes over time in relative abundance of hexose and pentose HGs present in Black Sea core 64PE418

Table 1: Outline of the seven ^{14}C dates used in the production of the age-model for core 64PE418 and their calibrated ages. The ^{14}C and calibrated age of 142.5 cm is shown but was excluded from the age-depth model due to an age reversal.

Core	Depth (cm)	Material	Radiocarbon age (^{14}C yr BP)	± 1σ	Calendar age (cal yr BP)	± 2σ
64PE418[a]	24.5	TOC	2010	30	435[c,e]	115
KNR134-08-BC17[b]	39.0	TOC	3640	70	2145[c,e]	205
64PE418[a]	76.5	TOC	5795	35	4870[c,e]	170
64PE418[a]	118.5	TOC	9110	50	9328[d,f]	128
64PE418[a]	*142.5*	*TOC*	*11650*	*60*	*12720[d,g]*	*50*
64PE418[a]	158.5	TOC	9670	50	9975[d,f]	205
64PE418[a]	183.5	TOC	12380	70	13358[d,g]	123
64PE418[a]	217.5	TOC	17420	110	19270[d,h]	250

a 14C dates from this study
b 14C dates from Jones & Gagnon, 1994
c Calibrated with the Marine20 curve (Heaton et al., 2020)
d Calibrated with the IntCal20 curve (Reimer et al., 2020)
e R-age of 600 years applied (Kwiecien et al., 2008)
f R-age of 800 years applied (Kwiecien et al., 2008)
g R-age of 900 years applied (Kwiecien et al., 2008)
h R-age of 1450 years applied (Kwiecien et al., 2008)